Translational regulation enhances distinction of cell types in the nervous system

Authors:

Toshiharu Ichinose[1,2,*], Shu Kondo[3], Mai Kanno[2], Yuichi Shichino[4], Mari Mito[4], Shintaro Iwasaki[4,5], Hiromu Tanimoto[2,*].

Affiliations:

1: Frontier Research Institute for Interdisciplinary Sciences, Tohoku University; 2: Graduate School of Life Sciences, Tohoku University; 3: Faculty of Advanced Engineering, Tokyo University of Sciences; 4: RNA Systems Biochemistry Laboratory, RIKEN Cluster for Pioneering Research, Wako, Saitama 351-0198, Japan 5: Department of Computational Biology and Medical Sciences, Graduate School of Frontier Sciences, The University of Tokyo, Kashiwa, Chiba 277-8561, Japan.

Correspondence authors:

Hiromu Tanimoto (hiromut@m.tohoku.ac.jp) and Toshiharu Ichinose (toshiharu.ichinose.c1@tohoku.ac.jp)

Author Contributions:

TI, SK, and HT conceptualized the project; TI performed ribosome profiling and RNA-seq with the help of YS, MM, and SI; MK performed immunohistochemistry and fluorescent in-situ hybridization, and managed fly care; SK constructed the transgenic reporter strain; YS, MM, and SI contributed to reagents, protocols, and analytic tools; TI analyzed all data with the help of YS and SI; TI and HT wrote the manuscript; SK, YS and SI edited the manuscript.

Competing Interest Statement:

The authors declare no competing interest.

Major Subject Areas:

Neuroscience and Cell Biology

Abstract:

Multicellular organisms are composed of specialized cell types with distinct proteomes. While recent advances in single-cell transcriptome analyses have revealed differential expression of mRNAs, cellular diversity in translational profiles remains underinvestigated. By performing RNA-seq and Ribo-seq in genetically-defined cells in the *Drosophila* brain, we here revealed substantial posttranscriptional regulations that augment the cell-type distinctions at the level of protein expression. Specifically, we found that translational efficiency of proteins fundamental to neuronal functions, such as ion channels and neurotransmitter receptors, was maintained low in glia, leading to their preferential translation in neurons. Notably, distribution of ribosome footprints on these mRNAs exhibited a remarkable bias towards the 5′ leaders in glia. Using transgenic reporter strains, we provide evidence that the small upstream open reading frames (uORFs) in the 5' leader confer selective translational suppression in glia. Overall, these findings underscore the profound impact of translational regulation in shaping the proteomics for cell-type distinction and provide new insights into the molecular mechanisms driving cell-type diversity.

Introduction:

Gene expression is regulated both at the transcription and translation levels (Becker et al., 2018; Casas-Vila et al., 2017; Li et al., 2020; Liu et al., 2016; Schwanhäusser et al., 2011), and its heterogeneity defines the specialized morphologies and functions of cells. The *Drosophila* brain is a well-studied model tissue with a diverse array of cell types, classifiable by morphology, cell lineage, or gene expression (Scheffer et al., 2020; Zeng and Sanes, 2017). Recent advances in single-cell transcriptomics have identified groups of differentially expressed genes and provided an in-depth overview of transcriptional regulations (Croset et al., 2018; Davie et al., 2018; Li et al., 2022). While these inventories provided a powerful way to classify cell types, there have been cases falling short in explaining proteomic or morphological diversity (Lago-Baldaia et al., 2023; Li et al., 2020). Therefore, posttranscriptional regulations play pivotal roles in distinguishing cell-type specific proteomes.

Ribosome profiling or Ribo-seq, which is based on deep-sequencing of mRNA fragments protected by ribosomes from RNase treatment (ribosome footprints), has been a powerful approach to provide a genome-wide snapshot of protein synthesis ('translatome') (Ingolia et al., 2009). Application of this method, combined with transcriptome analysis, revealed multiple layers of translational regulation in cells. For example, this comparison allowed measurements

of translational efficiency (TE), which is quantified as the number of ribosome footprints on the coding sequence per mRNA, and discoveries of previously unannotated ORFs (Dunn et al., 2013; Ingolia et al., 2011, 2009; Zhang et al., 2018). While TE profiles have been reported to be variable among dissected animal tissues (Fujii et al., 2017; Wang et al., 2021; Zhang et al., 2018), differences in translational regulations among identified cell types remain unclear.

Applying ribosome profiling to *Drosophila* heads, we here examine the comprehensive landscape of translational profiles between neuronal and glial cells. Due to the size of the fly brain (~0.5 mm) and intricate intercellular adhesions among neurons and glia (Kremer et al., 2017), surgical separation is impractical. We thus biochemically purified ribosome-bound mRNAs through genetic tagging of ribosomes in target cells (Chen and Dickman, 2017; Sapkota et al., 2019; Scheckel et al., 2020; Thomas et al., 2012; You et al., 2021) and further performed Ribo-seq and RNA-seq. By this comparative transcriptome-translatome analyses, we suggest that differential translational programs enhance the distinction of protein synthesis between neuronal and glial cells.

Results:

Comparative transcriptome-translatome analyses reveal translational suppression of selective groups of proteins in the fly heads

To gain an overview of the translation status, we first applied conventional Ribo-seq in the whole fly head, and successfully monitored footprint distribution at a single-codon resolution (Figure 1A, see 'Materials and Methods' for technical details). The majority (96.2%) of ribosome footprints was mapped onto the annotated coding sequences (CDS), and its distribution displayed a clear 3-nt periodicity, reflecting the codon-wise movement (Figure 1B).

To compare transcriptome and translatome, we also performed RNA-seq from the same lysate (Figure 1A). As previously reported, the transcript level and the number of ribosome footprints did not always match, suggesting substantial posttranscriptional regulations (R^2 = 0.664; Figure 1C). For instance, while *Shaker* (*Sh*) and *Trehalase* (*Treh*), which encode a voltage-gated K^+ channel and an enzyme that hydrolyzes trehalose, respectively, were similar regarding transcript levels, far more ribosome footprints were detected on *Treh* (Figure 1D-E). We therefore measured translational efficiency (TE), ribosome footprints normalized by mRNA reads. TE was much higher for *Treh* than *Sh* (Figure 1F), and we found a striking genome-wide variability with more than 20-fold TE difference between the 5 and 95 percentiles (Figure 1G). Kyoto Encyclopedia of Genes and Genome (KEGG) pathway enrichment analysis

94 revealed that transcripts involved in fatty acid metabolism and proteasome are actively
95 translated (Figure 1H). In contrast, ribosome proteins, as previously reported (Chen and
96 Dickman, 2017; Cho et al., 2015), and proteins mediating neuronal ligand-receptor interactions
97 were significantly enriched in the transcripts with low TE, suggesting translational suppression
98 (Figure 1H). Indeed, many transcripts encoding ligand- or voltage-gated ion channels, G-
99 protein coupled receptors (GPCR) showed remarkably low TE (Figure 1C and 1I). These
100 results suggest translational regulations specific to neuronal transcripts in the fly head.

101 **Translational regulation enhances the difference in the gene expression profiles**
102 **between cell types**

103 Because the translatome/transcriptome status of the whole heads was a mixed average
104 of diverse cell types, such as neurons, glial cells, fat bodies, and muscles, we set up an
105 experimental approach to dissect cell-type specific translational regulations. By expressing
106 epitope-tagged RpL3 (uL3 in universal nomenclature) (Chen and Dickman, 2017) under the
107 control of UAS using the *nSyb*- or the *repo-GAL4* drivers, we immunopurified the tagged
108 ribosomes and associated mRNAs separately from neurons and glia, and performed Ribo-seq
109 (Figure 2A). By immunohistochemistry, we confirmed that *UAS-RpL3::FLAG* on the third
110 chromosome exhibited minimum leakage expression in the brain and did not display any
111 apparent morphological defects upon expression using either driver, compared to other
112 insertions or constructs (Chen and Dickman, 2017; Huang et al., 2019; Thomas et al., 2012)
113 (Figures 2A and Figure 2 – figure supplement 1A-B). The exogenously expressed RpL3::FLAG
114 was highly concentrated in cell bodies but also detectable in neurites, consistent with the
115 subcellular localization of the endogenous ribosome (Figure 2 – figure supplement 1C-D).

116 Through the purification of FLAG-tagged ribosomes, we successfully profiled translatome
117 from neurons and glial cells in the fly heads: Footprints were found on 10,821 (78.4 % of all
118 the annotated genes) and 10,994 (79.7 %) genes in neurons and glia, respectively, with decent
119 reproducibility among the biological replicates (R^2 > 0.9, Figure 2 – figure supplement 2A). The
120 FLAG-tagged RpL3 in the corresponding cells far exceeded the endogenous RpL3, as RpL3
121 reads were 7.8 and 42.7 times higher in neurons and glia, respectively, compared to the wild-
122 type whole-head samples (Figure 2 – figure supplement 2B). The known marker genes were
123 strongly enriched while non-target markers were depleted (Figures 2B and Figure 2 – figure
124 supplement 2C-D) (Croset et al., 2018; Davie et al., 2018; Li et al., 2022), and the KEGG
125 enrichment analysis showed significant enrichment of footprints on genes associated with the
126 known functions of these cell types (Figure 2 – figure supplement 2E). Interestingly, the KEGG

127 analysis also revealed that neurons exhibit a greater extent of protein synthesis related to
128 oxidative phosphorylation and mitochondrial ribosome proteins, while glial cells show higher
129 expression of proteins associated with glycolysis (Figure 2 – figure supplement 2E-F). These
130 findings support the glia-neuron lactate shuttle hypothesis, a recently proposed concept of
131 metabolic specialization (Mason, 2017; Volkenhoff et al., 2015). Furthermore, apart from the
132 annotated CDS, we detected clustered ribosome footprints on *Hsr-ω*, previously annotated as
133 a long non-coding RNA, strongly suggesting the synthesis of hitherto undescribed
134 polypeptides (Figure 2 – figure supplement 2G) (Singh, 2022). Altogether, the combination of
135 genetic labelling of ribosomes in selective cell types and Ribo-seq revealed the differential
136 translatome profiles in the fly heads.

137 To further examine translational regulation by calculating TE, we performed RNA-seq
138 from the same immunoprecipitated complexes, similar to Translating Ribosome Affinity
139 Purification (TRAP) (Heiman et al., 2008) (Figures 2A and Figure 2 – figure supplement 3A-
140 B). Because this approach relies on the 80S-ribosome-mRNA complex, we may miss mRNA
141 with little or no translation. Nevertheless, our transcriptome was similar to the sn-transcriptome
142 data (Li et al., 2022) (Figure 2 – figure supplement 3C). We identified groups of genes
143 undergoing neuron- or glia- specific translational regulations compared to the whole heads
144 (Figure 2 – figure supplement 4A). Genes mediating fatty acid metabolism and degradation,
145 for example, were actively translated in the whole head, but showed lower TE in neurons or in
146 glia (Figures 1H and 2C). Because many of these genes are highly expressed in the fat bodies
147 (Dobson et al., 2018), these results suggest selective translational enhancement in the fat
148 body. Strikingly, TE of genes involved in neuroactive ligand-receptor interaction was
149 significantly higher in neurons but lower in glia (Figure 2C-D), suggesting cell-type specific
150 translational regulation of these genes.

151 This differential translational regulation was highlighted in the weak TE correlation
152 between neurons and glia (R^2 = 0.534, Figure 2E). We found a genome-wide tendency that
153 genes transcribed less in glia are further suppressed at translation (Figure 2F). Specifically,
154 many functionally-characterized neuronal genes, such as voltage- or ligand- gated ion
155 channels, G-protein coupled receptors, neuropeptides and proteins for visual perception,
156 showed particularly lower TE in glia (Figures 2E, 2G-H and Figure 2 – figure supplement 4C).
157 For these genes, the distinction between neuronal and glial cells was much exaggerated at
158 the level of translation than at transcription (Figure 2H). Consistently on the genome-wide
159 scale, the inter-cell type correlation became weaker in Ribo-seq data compared to in RNA-seq
160 (R^2 = 0.59 vs. 0.81, Figure 2 – figure supplement 3B). Altogether, these data indicate

161 substantial contributions of translational regulation to shaping the cell-type specific protein
162 expression.

163 **Biased distribution of ribosomes toward upstream open reading frames of neural genes**
164 **in glial cells**

165 We next analyzed the distribution of ribosome footprints on the differentially translated
166 transcripts (DTT). Fat-body related genes showed lower TE in neurons compared to the whole
167 head (Figure 2C). Among these genes, we found a remarkable ribosomal accumulation on the
168 start codon specifically in neurons (Figure 3 – figure supplement 1A-B), as if the first round of
169 the elongation cycle was arrested in neurons. Through the reanalysis of the published RNA-
170 seq data (Dobson et al., 2018), we found that mRNAs showing strong ribosomal accumulation
171 on the start codons are highly abundant in the fat bodies (Figure 3 – figure supplement 1C).
172 On the other hand, DTTs suppressed in glial cells compared to neurons (defined as genes
173 with more than 10 times higher TE in neurons than in glia, n = 161), we noticed that glial
174 ribosome footprints were remarkably biased towards 5′ leaders (Figure 3A-B). Notably, this
175 pattern was not obvious on the genome-wide scale (Figure 3A-B). The high 5′ leader/CDS
176 ratio of ribosome footprints in glia was commonly observed on many transcripts with known
177 neuronal functions, such as *Rab3, Syt4, Arr1* and *Syn* (Figure 3D-E). Conversely, we observed
178 accumulated ribosome footprints on the 5′ leaders of several glial marker genes specifically in
179 neurons (Figure 3 – figure supplement 2). Altogether, these results suggest that the translation
180 of 5' leaders in selective mRNAs differentiates protein synthesis among cell types.

181 We reasoned translational downregulation via upstream open reading frames (uORFs) in
182 the 5′ leaders in glia, as the translation of uORFs was reported to suppress that of the
183 downstream main ORF (Ferreira et al., 2013; Zhang et al., 2019, 2018). Consistent with this
184 idea, metagene plot around the AUG codons on 5′ leaders revealed strong accumulation of
185 footprints on the upstream AUG codons, similar to those observed on the initiation codon of
186 CDSs (Figures 4A-B). We calculated the footprint accumulation score on each codon (defined
187 as the ratio of footprints on each codon with surrounding -50/+50 nt), and found that upstream
188 AUG and the near cognate codons (NUG or AUN) showed relatively high accumulation (Figure
189 4C). On the other hand, inside the annotated CDS, none of the codons exhibited such
190 significant accumulation (Figures 4D). Consistently, we found that transcripts related to
191 neuronal functions typically contain long 5′ leaders and many upstream AUG (Figure 4 – figure
192 supplement 1). We thus propose that glial cells suppress the translation of neuronal transcripts
193 by stalling ribosomes on 5′ leader via uORF.

194 **uORFs in *Rh1* confer translational suppression in glia**

195 We next asked if the 5′ leader sequences of neuronal genes cause cell-type differences
196 in translation. To this end, we focused on *Rh1* (*Rhodopsin 1*, also known as *ninaE*), which
197 encodes an opsin, also detecting stimuli of other sensory modalities (Leung et al., 2020;
198 O'Tousa et al., 1985; Shen et al., 2011; Zuker et al., 1985). Consistently, active translation of
199 Rh1 was almost exclusively observed in neurons (Figure 5A). Similar to other neuronal genes
200 shown in Figure 3C, the distribution of ribosome footprints was distinct among neuronal and
201 glial cells: they were heavily biased to 5′ leader in glia, with the striking accumulation on the
202 putative uORFs composed only of the start and stop codons (Figure 5B-C).

203 To address the function of these sequences on differential traslation, we constructed a
204 transgenic reporter strain using the *Rh1* UTR sequences under the control of UAS (Figure 5D),
205 and directed gene expression ubiquitously using *Tub-GAL4*. While the reporter mRNA was
206 detected both in neuronal and glial cells, the protein levels were much more heterogeneous
207 and strikingly weak in glia (Figure 5E; Figure 5 – figure supplement 1A). The control reporter
208 strain (DeLuca and Spradling, 2018), on the other hand, exhibited more ubiquitous expression,
209 with significantly higher fluorescent intensity in glia (Figure 5E-F). Driving the reporter
210 expression using the *nSyb*- or *repo-GAL4* further corroborated cell-type specific suppression
211 in glia (Figure 5 – figure supplement 1B-C). Strikingly, when the 6-base putative uORFs were
212 mutated, the in-vivo protein-to-mRNA ratio of the reporter was significantly increased in glia
213 but not in neurons (Figure 5G-H). Based on these results, we propose that glial cells selectively
214 suppress the protein synthesis of neuronal genes through uORF and thereby enhance the
215 translatome distinction from neurons.

216

217 **Discussion:**

218 In this study, the comparative translatome-transcriptome analyses in the whole heads,
219 neurons and glial cells revealed the significant diversity of translational regulations across
220 different cell types. Particularly noteworthy was the differential translation of transcripts
221 encoding neuronal proteins, including ion channels and neurotransmitter receptors (Figure 2).
222 These neuronal transcripts exhibited preferential translation in neurons (Figure 2), and the
223 relatively long 5′ UTR of these transcripts strongly stalled ribosomes in glia (Figures 3, 4 and
224 Figure 4 – figure supplement 1). This characteristic feature of long 5′ leaders containing
225 numerous uORFs is also observed in neuronal transcripts in mammals (Glock et al., 2021).
226 While the 5′ leader-mediated translational regulations are known to be critical for quick

227 response to environmental changes, such as starvation or oxidative stress (Harding et al.,
228 2003; Mueller and Hinnebusch, 1986; Young and Wek, 2016), our study sheds light on its roles
229 in contrasting protein expression among cell types. Furthermore, considering a pivotal role of
230 *de novo* protein synthesis for long-lasting adaptation (Flexner et al., 1963; Tully et al., 1994),
231 it is plausible that similar mechanisms are employed for neuronal plasticity as well.

232 The next obvious question would be how the translation of neuronal transcripts is
233 differentiated among neuronal and glial cells. Ribosomes can initiate translation at uORFs
234 more frequently in glia. Alternatively, the post-termination 40S subunits reinitiate translation of
235 the coding sequence more often in neurons. These two possibilities can be distinguished by
236 profiling the rates of initiation or reinitiation, achievable through sequencing the footprints of
237 the 40S subunits, known as translation complex profile sequencing, coupled with conventional
238 Ribo-seq (Archer et al., 2016; Bohlen et al., 2020; Wagner et al., 2020). Although there are
239 various technical challenges, the application of this technique to specific cells within the brain
240 would elucidate these possibilities. Furthermore, previous studies have identified eIF1, eIF2α
241 kinases, and DENR/MCT1, as facilitators of translation of main ORF whose 5′ leaders harbor
242 uORFs (Ivanov et al., 2010; Schleich et al., 2014; Sonenberg and Hinnebusch, 2009; Zhou et
243 al., 2020). Interestingly, all these proteins are expressed more in neurons than in glia in our
244 dataset (supplementary table 1). Selective activation of these molecular machineries might
245 underlie the cell type specific translation.

246 Our cell-type specific translatome analysis further revealed translational regulations
247 beyond 5′ leaders. We found a remarkable ribosomal stall at the initiation codon in several
248 transcripts, a phenomenon observed in neurons but not in the entire heads (Figure 3 – figure
249 supplement 1). These transcripts are known to be massively expressed in the fat bodies but
250 less in the nervous system (Figure 3 – figure supplement 1C) (Dobson et al., 2018), and the
251 translation was further suppressed in neurons (Figure 3 – figure supplement 1). Therefore,
252 transition from initiation to elongation may serve as another regulatory checkpoint of protein
253 synthesis (Harnett et al., 2022; Wang et al., 2019), which enhances cell-type distinctions.
254 Furthermore, we found ribosome footprints also on the 3′ UTR of certain transcripts, such as
255 *Synapsin* (Figure 3C). Stop-codon readthrough has been reported to be more frequent in
256 neurons than in other cell types (Hudson et al., 2021; Karki et al., 2022; Prieto-Godino et al.,
257 2016). Because the readthrough events extend the protein C-terminus, its regulation can add
258 yet another layer of cell-type diversity (Dunn et al., 2013; Jungreis et al., 2011; Klagges et al.,
259 1996). Altogether, we here propose that translational regulations further differentiate
260 transcriptome distinctions, thereby shaping the cellular identity.

261 Due to the specialized functions of neuronal and glial cells, they express distinct sets of
262 proteins. Neurons allocate more ribosomes to proteins related to neurotransmission, visual
263 sensing and oxidative phosphorylation, while glial cells synthesize transporters and enzymes
264 for metabolism of amino acid, fatty acid or carbohydrates (Figure 2 – figure supplement 1F).
265 Despite these clear differences and specialization, a significant amount of neuronal and glial
266 cells has a common developmental origin. They originate from a stem cell lineage known as
267 neuro-glioblasts (Lai and Lee, 2006; Viktorin et al., 2011), and the fate of these cells can be
268 altered by the expression of a single gene, *glial cells missing* (*gcm*) (Hartenstein, 2011; Hosoya
269 et al., 1995). Therefore, translational regulations, in addition to transcriptional diversity, may
270 play a particularly important role in these sister cell types with distinct physiological roles.

271 In the *Drosophila* brain, approximately 100 stem cell lineages diverge into more than
272 5,000 morphologically distinct cell types (Ito et al., 2013; Scheffer et al., 2020; Yu et al., 2013).
273 Hence, translational regulations similar to those described in this study, or other possible
274 regulations, may play significant roles in further differentiating neuronal or glial subtypes.
275 Consistent with this idea, our *UAS-Rh1-Venus* reporter showed heterogeneous expression
276 even among neurons, contrasting with the more uniform expression observed in the control
277 *UASz-GFP* reporter (Figures 5E and Figure 5 – figure supplement 1B-C). In accordance,
278 choline acetyltransferase (ChAT), an enzyme needed to synthesize acetylcholine, and
279 vesicular acetylcholine transporter (VAChT) are transcribed in many glutamatergic and
280 GABAergic neurons but its protein synthesis is inhibited (Chen et al., 2023; Lacin et al., 2019).
281 Substantial post-transcriptional regulations are also implicated during development (Li et al.,
282 2020; Zhang et al., 2016). Taken together, multiple layers of transcriptional and
283 posttranscriptional regulations should shape the proteome diversity of cell types in the nervous
284 system. Further comparative transcriptome-translatome analyses using more specific GAL4
285 drivers should highlight the diversity of translational regulations leveraged in the brain.

286

287 **Limitation of the study:**

288 Because our cell-type specific Ribo-seq and RNA-seq are based on immunoprecipitation of
289 genetically tagged RpL3 (Chen et al., 2017), the read counts could contain biases, such as
290 underestimation of mRNA level with little or no translational activity, or over- and under-
291 representation of certain cell types originating from the heterogeneous expression of the
292 drivers.

293

294 **Materials and Methods:**

295 **Fly culture and genetics**

296 The flies were reared in a mass culture at 24 ºC under the 12-12 hour light-dark cycles on
297 the standard cornmeal food. The *Canton-S* strain was used as the wild-type. We utilized the
298 following transgenic strains: *w^{1118};;GMR57C10-GAL4* (*nSyb-GAL4*; BDSC #39171),
299 *w^{1118};;repo-GAL4* (BDSC #7415), *y^1w^{1118};;tublin-GAL4* (BDSC #5138), *w^{1118};MB010B* (BDSC
300 #68293), *w^{1118};;UAS-RpL3::FLAG* (BDSC #77132) (Chen and Dickman, 2017), *y^1v^1;UAS-Rh1-*
301 *Venus* (made in this study; see below), *y^1v^1;UAS-m-Rh1-Venus* (made in this study), *w;UASz-*
302 *GFP* (a kind gift from Dr. Steven DeLuca) (DeLuca and Spradling, 2018). Females of the GAL4
303 drivers were crossed to males of the UAS effectors, and the F1 progenies were used for the
304 experiments. Of note, although *UAS-EGFP::RpL10Ab* (Thomas et al., 2012) has been used to
305 isolate ribosomes from specific cells, its expression using the *repo-GAL4* caused lethality in
306 our hands.

307 **Library preparation for ribosome profiling**

308 *Tissue collection and lysate preparation*

309 Four to eight days old flies with mixed gender were flash-frozen with liquid nitrogen,
310 thoroughly vortexed, and the heads were isolated from the bodies with metal mesh in a similar
311 manner reported previously (Sun et al., 2020). Approximately 500 frozen heads were mixed
312 with 400 µl of frozen droplets of lysis buffer [20 mM Tris-HCl pH7.5, 150mM NaCl, 5 mM $MgCl_2$,
313 1 mM dithiothreitol, 1 % Triton X-100, 100 µg/ml chloramphenicol, and 100 µg/ml
314 cycloheximide] in a pre-chilled container, then pulverized with grinding at 3,000 rpm for 15
315 seconds using a Multi-beads Shocker (YASUI KIKAI). Cycloheximide and chroramphenicol
316 were added to the lysis buffer to prevent possible elongation and run-off of cytosolic and
317 mitochondrial ribosomes, respectively. The lysate was slowly thawed at 4 °C and the
318 supernatant was recovered after spinning down by a table top micro centrifuge. The lysate
319 was treated with 10 U of Turbo DNase (ThermoFisher Scientific) on ice for 10 min to digest
320 the genome DNA. The supernatant was further clarified by spinning at 20,000 g for 10 minutes.

321 *Immunoprecipitation*

322 Anti-FLAG M2 antibody (F1804, Sigma Aldrich) and Dynabeads M-280 bound to anti-
323 mouse IgG antibody (11201D, Invitrogen) were used for immunoprecipitation. 25 µl of the
324 beads solution, washed twice with the aforementioned lysis buffer, was mixed with 2.5 µl of
325 the M2 antibody, and incubated at 4 °C for 1 hour with rotation. Beads were incubated with the

326 lysate at 4 °C for 1 hour with rotation and washed for four times with the lysis buffer. The
327 ribosome-bound mRNA was eluted with 50 µl of 100 µg/ml 3× FLAG peptide (GEN-3XFLAG-
328 25, Protein Ark) dissolved in the lysis buffer.

329 *RNase digestion and library preparation*

330 Ribosome profiling was performed as described previously (McGlincy and Ingolia, 2017;
331 Mito et al., 2020) with modifications. We used RNase I from *E. coli* (N6901K, Epicentre) to
332 digest the crude (Figures 1, Figure 2 – figure supplement 1C-D) or the immunoprecipitated
333 (Figure 2) lysate. Concentration of RNA in lysate was measured with Qubit RNA HS kit
334 (Q32852, Thermo Fisher Scientific). RNase I was added at a dose of 0.25 U per 1 µg RNA in
335 a 50 µl reaction mixture, which was incubated at 25 °C for 45 minutes. We used 1.36 µg and
336 0.5 µg RNA to prepare the whole head libraries (Figures 1, Figure 2 – figure supplement 1C-
337 D) and the cell-type specific libraries (Figure 2-3), respectively. The RNase digestion was
338 stopped by adding 20 U of SUPERase•In (AM2694, ThermoFisher Scientific). Ribosomes
339 were isolated by MicroSpin S-400 HR columns (27-5140-01, GE Healthcare). Subsequently,
340 we purified RNA using the TRIzol-LS (10296010, ThermoFisher Scientific) and Direct-zol RNA
341 Microprep kit (R2062, Zymo Research), and isolated the RNA fragment ranging 17 to 34 nt by
342 polyacrylamide gel electrophoresis.

343 The isolated RNA fragments were ligated to custom-made preadenylated linkers
344 containing unique molecular identifiers and barcodes for library pooling, using T4 RNA ligase
345 2, truncated KQ (M0373L, New England Biolabs) (Mito et al., 2020). Ribosomal RNA was
346 depleted by hybridizing to the custom-made biotinylated 2′-*O*-methyl oligonucleotides with
347 complementary sequences to the *Drosophila* rRNA (see *Supplementary Method* for the
348 sequences), which can be pulled-down using the streptavidin-coated beads (65001,
349 ThermoFisher Scientific). The rRNA-depleted samples were reverse-transcribed with
350 ProtoScript II (M0368L, New England Biolabs), circularized with CircLigase II (CL9025K,
351 Epicentre), and PCR-amplified using Phusion polymerase (M0530S, New England Biolabs)
352 (Mito et al., 2020). The libraries were sequenced with the Illumina HiSeq 4000 system
353 (Illumina) with single-end reads of 50 bases.

354 **Library preparation for transcriptome analysis**

355 The crude (Figure 1) or the immunoprecipitated (Figure 2) lysate was prepared using the
356 same protocol as described above, but without RNase digestion. RNA was purified using
357 TRIzol-LS. The libraries were constructed in Azenta Japan Corporation, using the NEBNext
358 Poly(A) mRNA Magnetic Isolation Module (E7760, New England Biolabs) and MGIEasy RNA

359 Directional Library Prep kit (1000006386, MGI tech). Briefly, poly-A tailed mRNAs were
360 enriched with the oligo dT beads, fragmented, and reverse-transcribed using random primers.
361 After the second strand cDNA was synthesized, an adapter sequence was added. DNA library
362 was PCR-amplified. The libraries were sequenced with DNB-seq (MGI tech) with an option of
363 paired end reads for 150 bases.

364 **Data analysis**

365 Adaptor sequences were removed using Fastp (Chen et al., 2018), and the reads that
366 matched to the non-coding RNA were discarded. The remaining reads were mapped onto the
367 *Drosophila melanogaster* release 6 genome. Mapping was performed using STAR (Dobin et
368 al., 2013). PCR-duplicated reads were removed by referring to the unique molecular identifiers.
369 The number of uniquely mapped reads are as follows:

370 Ribo-seq:

Sample	#Reads
Canton-S, whole heads	1,427,090
nSyb-GAL4/UAS-RpL3::FLAG, after IP, replicate 1	2,443,467
nSyb-GAL4/UAS-RpL3::FLAG, after IP, replicate 2	1,135,284
repo-GAL4/UAS-RpL3::FLAG, after IP, replicate 1	2,698,259
repo-GAL4/UAS-RpL3::FLAG, after IP, replicate 2	2,133,920
nSyb-GAL4/UAS-RpL3::FLAG, whole heads, replicate 1	2,147,092
nSyb-GAL4/UAS-RpL3::FLAG, whole heads, replicate 2	2,361,588
repo-GAL4/UAS-RpL3::FLAG, whole heads, replicate 1	1,372,502
repo-GAL4/UAS-RpL3::FLAG, whole heads, replicate 2	1,846,122

371

372 RNA-seq:

Sample	#Reads
Canton-S, whole heads	29,132,939
nSyb-GAL4/UAS-RpL3::FLAG, after IP, replicate 1	40,638,850
nSyb-GAL4/UAS-RpL3::FLAG, after IP, replicate 2	34,247,848
repo-GAL4/UAS-RpL3::FLAG, after IP, replicate 1	30,906,375

repo-GAL4/UAS-RpL3::FLAG, after IP, replicate 2 31,928,337

373

374 For Ribo-seq analysis, fragments ranging from 20 to 34 nt for whole head samples and
375 21 to 36 nt for immunoprecipitated samples were used. For the whole head samples, the
376 position of the P site was estimated as 12 or 13 nt downstream from the 5′ end, for the 20 to
377 31 nt or 32-34 nt fragments, respectively (Ingolia et al., 2009). For the immunoprecipitated
378 samples, it was estimated as 12 or 13 nt downstream for the 21 nt or 22-36 nt fragments,
379 respectively. Footprints were considered to be on the CDS if the estimated P site was between
380 the annotated start and stop codons. RNA-seq analysis included all fragments greater than 30
381 nt in length. For genes with alternatively spliced transcripts, the isoform with the highest TPM
382 in the wild type RNA-seq sample (Figure 1) was selected as the 'representative' isoform. If not
383 specified, only the representative isoforms were considered. TE was calculated as TPM of
384 ribosome footprints on CDS divided by TPM of RNA-seq.

385 The KEGG-enrichment analyses were performed using iPAGE (Figures 1H and 2D)
386 (Goodarzi et al., 2009) or DAVID (Figure 2 – figure supplement 2E and Figure 2 – figure
387 supplement 4A) (Dennis et al., 2003). Statistical tests were performed with GraphPad Prism
388 9.

389 For the Fly Cell Atlas data (Figure 2 – figure supplement 3C), expression level was
390 calculated as the mean RPKM in all cells annotated as neuronal or glial cells in heads (Li et
391 al., 2022).

392 **Reporter construct and the transgenic strain**

393 DNA fragments containing a minimal hsp70 promoter (hsp70Bb) (DeLuca and Spradling,
394 2018), the 5′ leader or the mutated 5' leader of *Rh1-RA*, the first 15 bases of the CDS of *Rh1-*
395 *RA*, the Venus yellow fluorescent protein gene, and the 3′ UTR of *Rh1-RA* were synthesized
396 and cloned into the pBFv-UAS3 plasmid (Addgene #138399). The sequence of the resultant
397 plasmid is provided in the *Supporting Information Text*. The plasmid was then injected into y^1
398 v^1 *P{nos-phiC31}; P{CaryP}attP40,* and their progenies were screened for a *v*+ phenotype. A
399 single transformant was crossed to y^1 cho^2 v^1*; Sp/CyO* balancer to establish a transgenic line.

400 **Immunohistochemistry and fluorescent in-situ hybridization**

401 Immunohistochemistry (Figures 2A and Figure 2 – figure supplement 1) was performed
402 as previously described with minor modifications (Kanno et al., 2021). Briefly, dissected male
403 fly brains were fixed in 2 % paraformaldehyde in PBS for 1 hour at room temperature, washed

404 three times with PBST (0.1 % Triton X-100 in PBS), blocked with 3 % goat serum in PBST for
405 30 minutes, then incubated with the primary antibody solution at 4 ºC overnight (mouse anti-
406 FLAG (1:1000; Sigma-Aldrich; F1804), mouse anti-RpS6 (1:200; Cell Signaling; 54D2), and
407 rat anti-elav (1:20; DSHB; 7E8A10)). Subsequently, the brains were washed three times with
408 PBST, incubated with the secondary antibody solution at 4 ºC overnight (anti-mouse Alexa
409 Fluor 488 (1:400; Invitrogen; A11001), anti-mouse Cy3 (1:1000; Jackson ImmunoResearch;
410 115-166-003), and anti-rat Cy3 (1:200; Jackson ImmunoResearch; 112-166-003)), washed
411 three times with PBST and mounted with 86 % glycerol in PBS.

412 Fluorescent in-situ hybridization, combined with immunohistochemistry, was performed in
413 a similar manner to (Yang et al., 2017) with several modifications (Figure 5E-H). Dissected
414 male fly brains were fixed in PBS containing 3 % formaldehyde, 1 % glyoxal and 0.1 %
415 methanol for 30 min at room temperature, followed by three quick washes with PBT (0.5 %
416 Triton X-100 in PBS). Consistent with the previous study, the addition of glyoxal to the fixative
417 improved the FISH signal (Yao et al., 2021). The buffer was then exchanged to the wash
418 solution (10 % Hi-Di™ Formamide (Thermofisher scientific; 4311320) in 2x saline sodium
419 citrate (SSC)) and was incubated at 37 ºC for 5 minutes. Subsequently, the brains were
420 incubated with the custom-made Stellaris *Venus* or *GFP* probes (100 nM; see *Supporting*
421 *Information Text* for the sequences; LGC BioSearch Technologies) and the primary antibody
422 (mouse anti-Repo (1:100; DSHB; 8D12)) in the hybridization buffer (10% Hi-Di™ Formamide
423 in hybridization buffer (Stellaris RNA FISH Hybridization Buffer, SMF-HB1-10)) at 37 ºC for 16
424 hours. The probes and the antibody were then removed by washing the samples quickly three
425 times with preheated wash solution at 37 ºC, followed by three washes for 10 minutes at room
426 temperature. Blocking was performed with 3 % normal goat serum in PBT for 30 min at room
427 temperature. The secondary antibody (Cy3 goat anti-mouse (1:2000; Jackson
428 ImmunoResearch; 115-166-003)) was then added and was incubated at 4 ºC overnight. The
429 samples were washed once quickly, three times for 20 minutes, and once for 60 minutes with
430 PBT, and then mounted in 86 % glycerol in 1x Tris-HCl buffer (pH7.4).

431 Tissues to detect native GFP or Venus signals (Figure 5 – figure supplement 1) were
432 prepared as follows: dissected brains were fixed in PBS containing 3 % formaldehyde, 1 %
433 glyoxal and 0.1 % methanol for 30 min at room temperature, followed by one quick wash and
434 three washes for 10 minutes with PBT. The samples were then mounted in 86 % glycerol in
435 1x Tris-HCl buffer (pH7.4).

436 **Imaging and microscopes**

437 Imaging was done on the Olympus FV1200 confocal microscope with GaAsP sensors. A
438 100x/1.35 silicone immersion objective (UPLSAPO100XS, Olympus) or 30x/1.05 silicone
439 immersion objective (UPLSAPO30XS) was used. Scan settings were kept constant across
440 specimens to be compared.

441 **Data availability**

442 The raw sequence data were deposited in the National Center for Biotechnology
443 Information (NCBI) database with the project code (PRJNA992629). The custom scripts are
444 available in Zenodo (https://zenodo.org/records/10637789).

445

446 **Acknowledgments:**
447 We thank Dr. Steven DeLuca (Brandeis University), Dr. Atsushi Sugie (Niigata University),
448 and Dr. Yohei Nitta (Niigata University) for kindly providing the transgenic flies. We also thank
449 Dr. Yusuke Kimura and Dr. Yukihide Tomari (The University of Tokyo) for designing the fly
450 rRNA-depletion probes, Dr. Jasper Janssens (ETH Zurich), Dr. Hongjie Li (Baylor College of
451 Medicine), Dr. Gert Hulselmans (KU Leuven) and Dr. Stein Aerts (KU Leuven) for technical
452 advice regarding analysis of the Fly Cell Atlas data, Ayako Abe (Tohoku University) for
453 technical assistance, Dr. Takashi Makino (Tohoku University) for critical discussion, Madoka
454 Ichinose for critical comments on the graphic design, and the HOKUSAI SailingShip
455 supercomputer facility at RIKEN for computational supports.

456 This study was supported by the Ministry of Education, Culture, Sports, Science and
457 Technology (MEXT): 21K06369 (to TI), 21H05713 (to TI), JP20H05784 (to SI), JP21K15023
458 (to YS), 22H05481 (to HT), 22KK0106 (to HT), 20H00519 (to HT); Japan Society for the
459 Promotion of Science (JSPS): 21K06369 (to TI), JP21K15023 (to YS); Japan Agency for
460 Medical Research and Development (AMED): JP23gm1410001 (to SI); Takeda Life Science
461 Research Grant (to TI); RIKEN-Tohoku Univ Science & Technology Hub Collaborative
462 Research Program (to TI and YS), "Biology of Intracellular Environments" (to SI), Special
463 Postdoctoral Researchers (to YS), and Incentive Research Projects (to YS), Tohoku University
464 Research Program "Frontier Research in Duo" (to HT).

465

466 **References:**

467 Archer, S.K., Shirokikh, N.E., Beilharz, T.H., Preiss, T., 2016. Dynamics of ribosome
468 scanning and recycling revealed by translation complex profiling. Nature 535, 570–574.
469 https://doi.org/10.1038/nature18647

470 Becker, K., Bluhm, A., Casas-Vila, N., Dinges, N., Dejung, M., Sayols, S., Kreutz, C.,
471 Roignant, J.-Y., Butter, F., Legewie, S., 2018. Quantifying post-transcriptional regulation
472 in the development of Drosophila melanogaster. Nat Commun 9, 4970.
473 https://doi.org/10.1038/s41467-018-07455-9

474 Bohlen, J., Fenzl, K., Kramer, G., Bukau, B., Teleman, A.A., 2020. Selective 40S
475 Footprinting Reveals Cap-Tethered Ribosome Scanning in Human Cells. Molecular Cell
476 79, 561-574.e5. https://doi.org/10.1016/j.molcel.2020.06.005

477 Casas-Vila, N., Bluhm, A., Sayols, S., Dinges, N., Dejung, M., Altenhein, T., Kappei, D.,
478 Altenhein, B., Roignant, J.-Y., Butter, F., 2017. The developmental proteome of
479 *Drosophila melanogaster*. Genome Res. 27, 1273–1285.
480 https://doi.org/10.1101/gr.213694.116

481 Chen, N., Zhang, Y., Rivera-Rodriguez, E.J., Yu, A.D., Hobin, M., Rosbash, M., Griffith,
482 L.C., 2023. Widespread posttranscriptional regulation of cotransmission. Sci. Adv. 9,
483 eadg9836. https://doi.org/10.1126/sciadv.adg9836

484 Chen, S., Zhou, Y., Chen, Y., Gu, J., 2018. fastp: an ultra-fast all-in-one FASTQ
485 preprocessor. Bioinformatics 34, i884–i890.
486 https://doi.org/10.1093/bioinformatics/bty560

487 Chen, X., Dickman, D., 2017. Development of a tissue-specific ribosome profiling
488 approach in Drosophila enables genome-wide evaluation of translational adaptations.
489 PLoS Genet 13, e1007117. https://doi.org/10.1371/journal.pgen.1007117

490 Cho, J., Yu, N.-K., Choi, J.-H., Sim, S.-E., Kang, S.J., Kwak, C., Lee, S.-W., Kim, J.,
491 Choi, D.I., Kim, V.N., Kaang, B.-K., 2015. Multiple repressive mechanisms in the
492 hippocampus during memory formation. Science 350, 82–87.
493 https://doi.org/10.1126/science.aac7368

494 Croset, V., Treiber, C.D., Waddell, S., 2018. Cellular diversity in the Drosophila
495 midbrain revealed by single-cell transcriptomics. eLife 7, e34550.
496 https://doi.org/10.7554/eLife.34550

497 Davie, K., Janssens, J., Koldere, D., De Waegeneer, M., Pech, U., Kreft, Ł., Aibar, S.,
498 Makhzami, S., Christiaens, V., Bravo González-Blas, C., Poovathingal, S., Hulselmans,
499 G., Spanier, K.I., Moerman, T., Vanspauwen, B., Geurs, S., Voet, T., Lammertyn, J.,
500 Thienpont, B., Liu, S., Konstantinides, N., Fiers, M., Verstreken, P., Aerts, S., 2018. A
501 Single-Cell Transcriptome Atlas of the Aging Drosophila Brain. Cell 174, 982-998.e20.
502 https://doi.org/10.1016/j.cell.2018.05.057

503 DeLuca, S.Z., Spradling, A.C., 2018. Efficient Expression of Genes in the *Drosophila*
504 Germline Using a UAS Promoter Free of Interference by Hsp70 piRNAs. Genetics 209,
505 381–387. https://doi.org/10.1534/genetics.118.300874

506 Dennis, G., Sherman, B.T., Hosack, D.A., Yang, J., Gao, W., Lane, H.C., Lempicki,
507 R.A., 2003. DAVID: Database for Annotation, Visualization, and Integrated Discovery.
508 Genome Biol 4, R60. https://doi.org/10.1186/gb-2003-4-9-r60

509 Dobin, A., Davis, C.A., Schlesinger, F., Drenkow, J., Zaleski, C., Jha, S., Batut, P.,
510 Chaisson, M., Gingeras, T.R., 2013. STAR: ultrafast universal RNA-seq aligner.
511 Bioinformatics 29, 15–21. https://doi.org/10.1093/bioinformatics/bts635

512 Dobson, A.J., He, X., Blanc, E., Bolukbasi, E., Feseha, Y., Yang, M., Piper, M.D.W.,
513 2018. Tissue-specific transcriptome profiling of Drosophila reveals roles for GATA
514 transcription factors in longevity by dietary restriction. npj Aging Mech Dis 4, 5.
515 https://doi.org/10.1038/s41514-018-0024-4

516 Dunn, J.G., Foo, C.K., Belletier, N.G., Gavis, E.R., Weissman, J.S., 2013. Ribosome
517 profiling reveals pervasive and regulated stop codon readthrough in Drosophila
518 melanogaster. eLife 2, e01179. https://doi.org/10.7554/eLife.01179

519 Ferreira, J.P., Overton, K.W., Wang, C.L., 2013. Tuning gene expression with synthetic
520 upstream open reading frames. Proc. Natl. Acad. Sci. U.S.A. 110, 11284–11289.
521 https://doi.org/10.1073/pnas.1305590110

522 Flexner, J.B., Flexner, L.B., Stellar, E., 1963. Memory in mice as affected by
523 intracerebral puromycin. Science 141, 57–59.
524 https://doi.org/10.1126/science.141.3575.57

525 Fujii, K., Shi, Z., Zhulyn, O., Denans, N., Barna, M., 2017. Pervasive translational
526 regulation of the cell signalling circuitry underlies mammalian development. Nat
527 Commun 8, 14443. https://doi.org/10.1038/ncomms14443

528 Glock, C., Biever, A., Tushev, G., Nassim-Assir, B., Kao, A., Bartnik, I., tom Dieck, S.,
529 Schuman, E.M., 2021. The translatome of neuronal cell bodies, dendrites, and axons.
530 Proc. Natl. Acad. Sci. U.S.A. 118, e2113929118.
531 https://doi.org/10.1073/pnas.2113929118

532 Goodarzi, H., Elemento, O., Tavazoie, S., 2009. Revealing Global Regulatory
533 Perturbations across Human Cancers. Molecular Cell 36, 900–911.
534 https://doi.org/10.1016/j.molcel.2009.11.016

535 Harding, H.P., Zhang, Y., Zeng, H., Novoa, I., Lu, P.D., Calfon, M., Sadri, N., Yun, C.,
536 Popko, B., Paules, R., Stojdl, D.F., Bell, J.C., Hettmann, T., Leiden, J.M., Ron, D., 2003.
537 An Integrated Stress Response Regulates Amino Acid Metabolism and Resistance to
538 Oxidative Stress. Molecular Cell 11, 619–633. https://doi.org/10.1016/S1097-
539 2765(03)00105-9

540 Harnett, D., Ambrozkiewicz, M.C., Zinnall, U., Rusanova, A., Borisova, E., Drescher,
541 A.N., Couce-Iglesias, M., Villamil, G., Dannenberg, R., Imami, K., Münster-Wandowski,
542 A., Fauler, B., Mielke, T., Selbach, M., Landthaler, M., Spahn, C.M.T., Tarabykin, V.,
543 Ohler, U., Kraushar, M.L., 2022. A critical period of translational control during brain
544 development at codon resolution. Nat Struct Mol Biol 29, 1277–1290.
545 https://doi.org/10.1038/s41594-022-00882-9

546 Hartenstein, V., 2011. Morphological diversity and development of glia in *Drosophila*.
547 Glia 59, 1237–1252. https://doi.org/10.1002/glia.21162

548 Heiman, M., Schaefer, A., Gong, S., Peterson, J.D., Day, M., Ramsey, K.E., Suárez-
549 Fariñas, M., Schwarz, C., Stephan, D.A., Surmeier, D.J., Greengard, P., Heintz, N., 2008.
550 A Translational Profiling Approach for the Molecular Characterization of CNS Cell
551 Types. Cell 135, 738–748. https://doi.org/10.1016/j.cell.2008.10.028

552 Hosoya, T., Takizawa, K., Nitta, K., Hotta, Y., 1995. Glial cells missing: A binary switch
553 between neuronal and glial determination in drosophila. Cell 82, 1025–1036.
554 https://doi.org/10.1016/0092-8674(95)90281-3

555 Huang, K., Chen, W., Zhu, F., Li, P.W.-L., Kapahi, P., Bai, H., 2019. RiboTag
556 translatomic profiling of Drosophila oenocytes under aging and induced oxidative stress.
557 BMC Genomics 20, 50. https://doi.org/10.1186/s12864-018-5404-4

558 Hudson, A.M., Szabo, N.L., Loughran, G., Wills, N.M., Atkins, J.F., Cooley, L., 2021.
559 Tissue-specific dynamic codon redefinition in *Drosophila*. Proc. Natl. Acad. Sci. U.S.A.
560 118, e2012793118. https://doi.org/10.1073/pnas.2012793118

561 Ingolia, N.T., Ghaemmaghami, S., Newman, J.R.S., Weissman, J.S., 2009. Genome-wide
562 analysis in vivo of translation with nucleotide resolution using ribosome profiling.
563 Science 324, 218–223. https://doi.org/10.1126/science.1168978

564 Ingolia, N.T., Lareau, L.F., Weissman, J.S., 2011. Ribosome Profiling of Mouse
565 Embryonic Stem Cells Reveals the Complexity and Dynamics of Mammalian Proteomes.
566 Cell 147, 789–802. https://doi.org/10.1016/j.cell.2011.10.002

567 Ito, M., Masuda, N., Shinomiya, K., Endo, K., Ito, K., 2013. Systematic Analysis of
568 Neural Projections Reveals Clonal Composition of the Drosophila Brain. Current Biology
569 23, 644–655. https://doi.org/10.1016/j.cub.2013.03.015

570 Ivanov, I.P., Loughran, G., Sachs, M.S., Atkins, J.F., 2010. Initiation context modulates
571 autoregulation of eukaryotic translation initiation factor 1 (eIF1). Proc. Natl. Acad. Sci.
572 U.S.A. 107, 18056–18060. https://doi.org/10.1073/pnas.1009269107

573 Jungreis, I., Lin, M.F., Spokony, R., Chan, C.S., Negre, N., Victorsen, A., White, K.P.,
574 Kellis, M., 2011. Evidence of abundant stop codon readthrough in *Drosophila* and other
575 metazoa. Genome Res. 21, 2096–2113. https://doi.org/10.1101/gr.119974.110

576 Kanno, M., Hiramatsu, S., Kondo, S., Tanimoto, H., Ichinose, T., 2021. Voluntary intake
577 of psychoactive substances is regulated by the dopamine receptor Dop1R1 in Drosophila.
578 Sci Rep 11, 3432. https://doi.org/10.1038/s41598-021-82813-0

579 Karki, P., Carney, T.D., Maracci, C., Yatsenko, A.S., Shcherbata, H.R., Rodnina, M.V.,
580 2022. Tissue-specific regulation of translational readthrough tunes functions of the traffic
581 jam transcription factor. Nucleic Acids Research 50, 6001–6019.
582 https://doi.org/10.1093/nar/gkab1189

583 Klagges, B.R.E., Heimbeck, G., Godenschwege, T.A., Hofbauer, A., Pflugfelder, G.O.,
584 Reifegerste, R., Reisch, D., Schaupp, M., Buchner, S., Buchner, E., 1996. Invertebrate
585 Synapsins: A Single Gene Codes for Several Isoforms in *Drosophila*. J. Neurosci. 16,
586 3154–3165. https://doi.org/10.1523/JNEUROSCI.16-10-03154.1996

587 Kremer, M.C., Jung, C., Batelli, S., Rubin, G.M., Gaul, U., 2017. The glia of the adult
588 *Drosophila* nervous system: Glia Anatomy in Adult Drosophila Nervous System. Glia
589 65, 606–638. https://doi.org/10.1002/glia.23115

590 Lacin, H., Chen, H.-M., Long, X., Singer, R.H., Lee, T., Truman, J.W., 2019.
591 Neurotransmitter identity is acquired in a lineage-restricted manner in the Drosophila
592 CNS. eLife 8, e43701. https://doi.org/10.7554/eLife.43701

593 Lago-Baldaia, I., Cooper, M., Seroka, A., Trivedi, C., Powell, G.T., Wilson, S.W.,
594 Ackerman, S.D., Fernandes, V.M., 2023. A Drosophila glial cell atlas reveals a mismatch
595 between transcriptional and morphological diversity. PLoS Biol 21, e3002328.
596 https://doi.org/10.1371/journal.pbio.3002328

597 Lai, S.-L., Lee, T., 2006. Genetic mosaic with dual binary transcriptional systems in
598 Drosophila. Nat Neurosci 9, 703–709. https://doi.org/10.1038/nn1681

599 Leung, N.Y., Thakur, D.P., Gurav, A.S., Kim, S.H., Di Pizio, A., Niv, M.Y., Montell, C.,
600 2020. Functions of Opsins in Drosophila Taste. Current Biology 30, 1367-1379.e6.
601 https://doi.org/10.1016/j.cub.2020.01.068

602 Li, H., Janssens, J., De Waegeneer, M., Kolluru, S.S., Davie, K., Gardeux, V., Saelens,
603 W., David, F.P.A., Brbić, M., Spanier, K., Leskovec, J., McLaughlin, C.N., Xie, Q.,
604 Jones, R.C., Brueckner, K., Shim, J., Tattikota, S.G., Schnorrer, F., Rust, K., Nystul,
605 T.G., Carvalho-Santos, Z., Ribeiro, C., Pal, S., Mahadevaraju, S., Przytycka, T.M., Allen,
606 A.M., Goodwin, S.F., Berry, C.W., Fuller, M.T., White-Cooper, H., Matunis, E.L.,
607 DiNardo, S., Galenza, A., O'Brien, L.E., Dow, J.A.T., FCA Consortium§, Jasper, H.,
608 Oliver, B., Perrimon, N., Deplancke, B., Quake, S.R., Luo, L., Aerts, S., Agarwal, D.,
609 Ahmed-Braimah, Y., Arbeitman, M., Ariss, M.M., Augsburger, J., Ayush, K., Baker,
610 C.C., Banisch, T., Birker, K., Bodmer, R., Bolival, B., Brantley, S.E., Brill, J.A., Brown,
611 N.C., Buehner, N.A., Cai, X.T., Cardoso-Figueiredo, R., Casares, F., Chang, A.,
612 Clandinin, T.R., Crasta, S., Desplan, C., Detweiler, A.M., Dhakan, D.B., Donà, E.,
613 Engert, S., Floc'hlay, S., George, N., González-Segarra, A.J., Groves, A.K., Gumbin, S.,
614 Guo, Y., Harris, D.E., Heifetz, Y., Holtz, S.L., Horns, F., Hudry, B., Hung, R.-J., Jan,

615 Y.N., Jaszczak, J.S., Jefferis, G.S.X.E., Karkanias, J., Karr, T.L., Katheder, N.S., Kezos,
616 J., Kim, A.A., Kim, S.K., Kockel, L., Konstantinides, N., Kornberg, T.B., Krause, H.M.,
617 Labott, A.T., Laturney, M., Lehmann, R., Leinwand, S., Li, J., Li, J.S.S., Li, Kai, Li, Ke,
618 Li, L., Li, T., Litovchenko, M., Liu, H.-H., Liu, Y., Lu, T.-C., Manning, J., Mase, A.,
619 Matera-Vatnick, M., Matias, N.R., McDonough-Goldstein, C.E., McGeever, A.,
620 McLachlan, A.D., Moreno-Roman, P., Neff, N., Neville, M., Ngo, S., Nielsen, T.,
621 O'Brien, C.E., Osumi-Sutherland, D., Özel, M.N., Papatheodorou, I., Petkovic, M.,
622 Pilgrim, C., Pisco, A.O., Reisenman, C., Sanders, E.N., dos Santos, G., Scott, K.,
623 Sherlekar, A., Shiu, P., Sims, D., Sit, R.V., Slaidina, M., Smith, H.E., Sterne, G., Su, Y.-
624 H., Sutton, D., Tamayo, M., Tan, M., Tastekin, I., Treiber, C., Vacek, D., Vogler, G.,
625 Waddell, S., Wang, W., Wilson, R.I., Wolfner, M.F., Wong, Y.-C.E., Xie, A., Xu, J.,
626 Yamamoto, S., Yan, J., Yao, Z., Yoda, K., Zhu, R., Zinzen, R.P., 2022. Fly Cell Atlas: A
627 single-nucleus transcriptomic atlas of the adult fruit fly. Science 375, eabk2432.
628 https://doi.org/10.1126/science.abk2432

629 Li, J., Han, S., Li, H., Udeshi, N.D., Svinkina, T., Mani, D.R., Xu, C., Guajardo, R., Xie,
630 Q., Li, T., Luginbuhl, D.J., Wu, B., McLaughlin, C.N., Xie, A., Kaewsapsak, P., Quake,
631 S.R., Carr, S.A., Ting, A.Y., Luo, L., 2020. Cell-Surface Proteomic Profiling in the Fly
632 Brain Uncovers Wiring Regulators. Cell 180, 373-386.e15.
633 https://doi.org/10.1016/j.cell.2019.12.029

634 Liu, Y., Beyer, A., Aebersold, R., 2016. On the Dependency of Cellular Protein Levels
635 on mRNA Abundance. Cell 165, 535–550. https://doi.org/10.1016/j.cell.2016.03.014

636 Mason, S., 2017. Lactate Shuttles in Neuroenergetics—Homeostasis, Allostasis and
637 Beyond. Front. Neurosci. 11. https://doi.org/10.3389/fnins.2017.00043

638 McGlincy, N.J., Ingolia, N.T., 2017. Transcriptome-wide measurement of translation by
639 ribosome profiling. Methods 126, 112–129. https://doi.org/10.1016/j.ymeth.2017.05.028

640 Mito, M., Mishima, Y., Iwasaki, S., 2020. Protocol for Disome Profiling to Survey
641 Ribosome Collision in Humans and Zebrafish. STAR Protocols 1, 100168.
642 https://doi.org/10.1016/j.xpro.2020.100168

643 Mueller, P.P., Hinnebusch, A.G., 1986. Multiple upstream AUG codons mediate
644 translational control of GCN4. Cell 45, 201–207. https://doi.org/10.1016/0092-
645 8674(86)90384-3

646 O'Tousa, J.E., Baehr, W., Martin, R.L., Hirsh, J., Pak, W.L., Applebury, M.L., 1985. The
647 Drosophila ninaE gene encodes an opsin. Cell 40, 839–850. https://doi.org/10.1016/0092-
648 8674(85)90343-5

649 Prieto-Godino, L.L., Rytz, R., Bargeton, B., Abuin, L., Arguello, J.R., Peraro, M.D.,
650 Benton, R., 2016. Olfactory receptor pseudo-pseudogenes. Nature 539, 93–97.
651 https://doi.org/10.1038/nature19824

652 Sapkota, D., Lake, A.M., Yang, W., Yang, C., Wesseling, H., Guise, A., Uncu, C., Dalal,
653 J.S., Kraft, A.W., Lee, J.-M., Sands, M.S., Steen, J.A., Dougherty, J.D., 2019. Cell-Type-
654 Specific Profiling of Alternative Translation Identifies Regulated Protein Isoform
655 Variation in the Mouse Brain. Cell Reports 26, 594-607.e7.
656 https://doi.org/10.1016/j.celrep.2018.12.077

657 Scheckel, C., Imeri, M., Schwarz, P., Aguzzi, A., 2020. Ribosomal profiling during prion
658 disease uncovers progressive translational derangement in glia but not in neurons. eLife
659 9, e62911. https://doi.org/10.7554/eLife.62911

660 Scheffer, L.K., Xu, C.S., Januszewski, M., Lu, Z., Takemura, Shin-ya, Hayworth, K.J.,
661 Huang, G.B., Shinomiya, K., Maitlin-Shepard, J., Berg, S., Clements, J., Hubbard, P.M.,
662 Katz, W.T., Umayam, L., Zhao, T., Ackerman, D., Blakely, T., Bogovic, J., Dolafi, T.,
663 Kainmueller, D., Kawase, T., Khairy, K.A., Leavitt, L., Li, P.H., Lindsey, L., Neubarth,
664 N., Olbris, D.J., Otsuna, H., Trautman, E.T., Ito, M., Bates, A.S., Goldammer, J., Wolff,
665 T., Svirskas, R., Schlegel, P., Neace, E., Knecht, C.J., Alvarado, C.X., Bailey, D.A.,
666 Ballinger, S., Borycz, J.A., Canino, B.S., Cheatham, N., Cook, M., Dreher, M., Duclos,
667 O., Eubanks, B., Fairbanks, K., Finley, S., Forknall, N., Francis, A., Hopkins, G.P.,
668 Joyce, E.M., Kim, S., Kirk, N.A., Kovalyak, J., Lauchie, S.A., Lohff, A., Maldonado, C.,
669 Manley, E.A., McLin, S., Mooney, C., Ndama, M., Ogundeyi, O., Okeoma, N., Ordish,
670 C., Padilla, N., Patrick, C.M., Paterson, T., Phillips, E.E., Phillips, E.M., Rampally, N.,
671 Ribeiro, C., Robertson, M.K., Rymer, J.T., Ryan, S.M., Sammons, M., Scott, A.K., Scott,
672 A.L., Shinomiya, A., Smith, C., Smith, K., Smith, N.L., Sobeski, M.A., Suleiman, A.,
673 Swift, J., Takemura, Satoko, Talebi, I., Tarnogorska, D., Tenshaw, E., Tokhi, T., Walsh,
674 J.J., Yang, T., Horne, J.A., Li, F., Parekh, R., Rivlin, P.K., Jayaraman, V., Costa, M.,
675 Jefferis, G.S., Ito, K., Saalfeld, S., George, R., Meinertzhagen, I.A., Rubin, G.M., Hess,
676 H.F., Jain, V., Plaza, S.M., 2020. A connectome and analysis of the adult Drosophila
677 central brain. eLife 9, e57443. https://doi.org/10.7554/eLife.57443

678 Schleich, S., Strassburger, K., Janiesch, P.C., Koledachkina, T., Miller, K.K., Haneke, K.,
679 Cheng, Y.-S., Küchler, K., Stoecklin, G., Duncan, K.E., Teleman, A.A., 2014. DENR–
680 MCT-1 promotes translation re-initiation downstream of uORFs to control tissue growth.
681 Nature 512, 208–212. https://doi.org/10.1038/nature13401

682 Schwanhäusser, B., Busse, D., Li, N., Dittmar, G., Schuchhardt, J., Wolf, J., Chen, W.,
683 Selbach, M., 2011. Global quantification of mammalian gene expression control. Nature
684 473, 337–342. https://doi.org/10.1038/nature10098

685 Shen, W.L., Kwon, Y., Adegbola, A.A., Luo, J., Chess, A., Montell, C., 2011. Function
686 of Rhodopsin in Temperature Discrimination in *Drosophila*. Science 331, 1333–1336.
687 https://doi.org/10.1126/science.1198904

688 Singh, A.K., 2022. Hsrω and Other lncRNAs in Neuronal Functions and Disorders in
689 Drosophila. Life 13, 17. https://doi.org/10.3390/life13010017

690 Sonenberg, N., Hinnebusch, A.G., 2009. Regulation of Translation Initiation in
691 Eukaryotes: Mechanisms and Biological Targets. Cell 136, 731–745.
692 https://doi.org/10.1016/j.cell.2009.01.042

693 Sun, H., Nishioka, T., Hiramatsu, S., Kondo, S., Amano, M., Kaibuchi, K., Ichinose, T.,
694 Tanimoto, H., 2020. Dopamine Receptor Dop1R2 Stabilizes Appetitive Olfactory
695 Memory through the Raf/MAPK Pathway in Drosophila. J. Neurosci. 40, 2935–2942.
696 https://doi.org/10.1523/JNEUROSCI.1572-19.2020

697 Thomas, A., Lee, P.-J., Dalton, J.E., Nomie, K.J., Stoica, L., Costa-Mattioli, M., Chang,
698 P., Nuzhdin, S., Arbeitman, M.N., Dierick, H.A., 2012. A Versatile Method for Cell-
699 Specific Profiling of Translated mRNAs in Drosophila. PLoS ONE 7, e40276.
700 https://doi.org/10.1371/journal.pone.0040276

701 Tully, T., Preat, T., Boynton, S.C., Del Vecchio, M., 1994. Genetic dissection of
702 consolidated memory in Drosophila. Cell 79, 35–47. https://doi.org/10.1016/0092-
703 8674(94)90398-0

704 Viktorin, G., Riebli, N., Popkova, A., Giangrande, A., Reichert, H., 2011. Multipotent
705 neural stem cells generate glial cells of the central complex through transit amplifying
706 intermediate progenitors in Drosophila brain development. Developmental Biology 356,
707 553–565. https://doi.org/10.1016/j.ydbio.2011.06.013

708 Volkenhoff, A., Weiler, A., Letzel, M., Stehling, M., Klämbt, C., Schirmeier, S., 2015.
709 Glial Glycolysis Is Essential for Neuronal Survival in Drosophila. Cell Metabolism 22,
710 437–447. https://doi.org/10.1016/j.cmet.2015.07.006

711 Wagner, S., Herrmannová, A., Hronová, V., Gunišová, S., Sen, N.D., Hannan, R.D.,
712 Hinnebusch, A.G., Shirokikh, N.E., Preiss, T., Valášek, L.S., 2020. Selective Translation
713 Complex Profiling Reveals Staged Initiation and Co-translational Assembly of Initiation
714 Factor Complexes. Molecular Cell 79, 546-560.e7.
715 https://doi.org/10.1016/j.molcel.2020.06.004

716 Wang, H., Wang, Y., Yang, J., Zhao, Q., Tang, N., Chen, C., Li, H., Cheng, C., Xie, M.,
717 Yang, Y., Xie, Z., 2021. Tissue- and stage-specific landscape of the mouse translatome.
718 Nucleic Acids Research 49, 6165–6180. https://doi.org/10.1093/nar/gkab482

719 Wang, J., Johnson, A.G., Lapointe, C.P., Choi, J., Prabhakar, A., Chen, D.-H., Petrov,
720 A.N., Puglisi, J.D., 2019. eIF5B gates the transition from translation initiation to
721 elongation. Nature 573, 605–608. https://doi.org/10.1038/s41586-019-1561-0

722 Yang, L., Titlow, J., Ennis, D., Smith, C., Mitchell, J., Young, F.L., Waddell, S., Ish-
723 Horowicz, D., Davis, I., 2017. Single molecule fluorescence in situ hybridisation for
724 quantitating post-transcriptional regulation in Drosophila brains. Methods 126, 166–176.
725 https://doi.org/10.1016/j.ymeth.2017.06.025

726 Yao, R.-W., Luan, P.-F., Chen, L.-L., 2021. An optimized fixation method containing
727 glyoxal and paraformaldehyde for imaging nuclear bodies. RNA 27, 725–733.
728 https://doi.org/10.1261/rna.078671.120

729 You, S., Yu, A.M., Roberts, M.A., Joseph, I.J., Jackson, F.R., 2021. Circadian regulation
730 of the Drosophila astrocyte transcriptome. PLoS Genet 17, e1009790.
731 https://doi.org/10.1371/journal.pgen.1009790

732 Young, S.K., Wek, R.C., 2016. Upstream Open Reading Frames Differentially Regulate
733 Gene-specific Translation in the Integrated Stress Response. Journal of Biological
734 Chemistry 291, 16927–16935. https://doi.org/10.1074/jbc.R116.733899

735 Yu, H.-H., Awasaki, T., Schroeder, M.D., Long, F., Yang, J.S., He, Y., Ding, P., Kao, J.-
736 C., Wu, G.Y.-Y., Peng, H., Myers, G., Lee, T., 2013. Clonal Development and
737 Organization of the Adult Drosophila Central Brain. Current Biology 23, 633–643.
738 https://doi.org/10.1016/j.cub.2013.02.057

739 Zeng, H., Sanes, J.R., 2017. Neuronal cell-type classification: challenges, opportunities
740 and the path forward. Nat Rev Neurosci 18, 530–546. https://doi.org/10.1038/nrn.2017.85

741 Zhang, H., Dou, S., He, F., Luo, J., Wei, L., Lu, J., 2018. Genome-wide maps of
742 ribosomal occupancy provide insights into adaptive evolution and regulatory roles of
743 uORFs during Drosophila development. PLoS Biol 16, e2003903.
744 https://doi.org/10.1371/journal.pbio.2003903

745 Zhang, H., Wang, Y., Lu, J., 2019. Function and Evolution of Upstream ORFs in
746 Eukaryotes. Trends in Biochemical Sciences 44, 782–794.
747 https://doi.org/10.1016/j.tibs.2019.03.002

748 Zhang, K.X., Tan, L., Pellegrini, M., Zipursky, S.L., McEwen, J.M., 2016. Rapid
749 Changes in the Translatome during the Conversion of Growth Cones to Synaptic
750 Terminals. Cell Reports 14, 1258–1271. https://doi.org/10.1016/j.celrep.2015.12.102

751 Zhou, F., Zhang, H., Kulkarni, S.D., Lorsch, J.R., Hinnebusch, A.G., 2020. eIF1
752 discriminates against suboptimal initiation sites to prevent excessive uORF translation
753 genome-wide. RNA 26, 419–438. https://doi.org/10.1261/rna.073536.119

754 Zuker, C.S., Cowman, A.F., Rubin, G.M., 1985. Isolation and structure of a rhodopsin
755 gene from D. melanogaster. Cell 40, 851–858. https://doi.org/10.1016/0092-
756 8674(85)90344-7

757
758

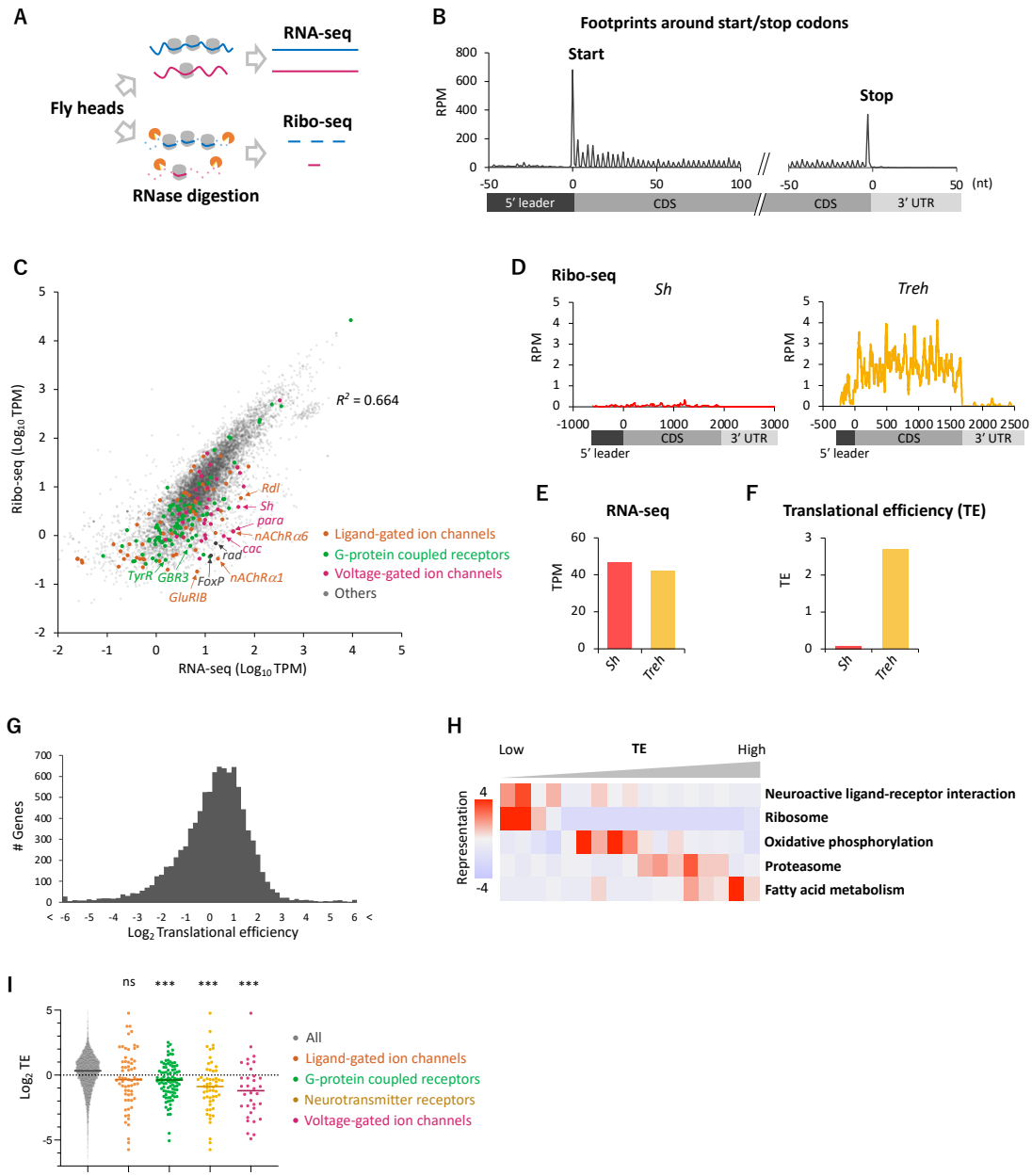

Figure 1. Comparative transcriptome-translatome analyses in the *Drosophila* head.

(A) Schematics. Fly head lysate is digested with RNase I for Ribo-seq, while not for RNA-seq. Resultant short fragments or the whole mRNA are reverse-transcribed and sequenced. (B) Meta-genome ribosome distribution (estimated P-sites of the 21-nt fragments), relative to the annotated start and stop codons. RPM: reads per million. (C) Scatter plots of mRNA reads (x-axis, TPM: transcripts per million) and ribosome footprints on CDS (y-axis, TPM). Several neuron-related genes are highlighted with colors and arrows. The squared Pearson's correlation coefficient (R^2) is indicated. (D-F) Ribosome footprints (D), mRNA level (E), and

768 translational efficiency (F) of *Shaker-RB* (*Sh*) and *Trehalase-RA* (*Treh*). TE: translational
769 efficiency. TE is calculated as ribosome footprints on CDS (TPM) divided by the mRNA level
770 (TPM). (G) Histogram of TE. The bin size is 0.2 in the unit of log 2. Total 9,611 genes with at
771 least one read in both Ribo-seq and RNA-seq are plotted. (H) Kyoto Encyclopedia of Genes
772 and Genomes (KEGG) pathways enrichment analysis, visualized by iPAGE (Goodarzi et al.,
773 2009), based on TE. The 9,611 genes are ranked and binned according to TE (left to right: low
774 to high), and over- and under- representation is tested. The presented KEGG pathways show
775 P values smaller than 0.0005. (I) TE of transcripts in the denoted gene ontology terms. Bars
776 represent the median. ns: $P > 0.05$; ***: $P < 0.001$; in the Dunn's multiple comparisons test,
777 compared to the "all" group.

778

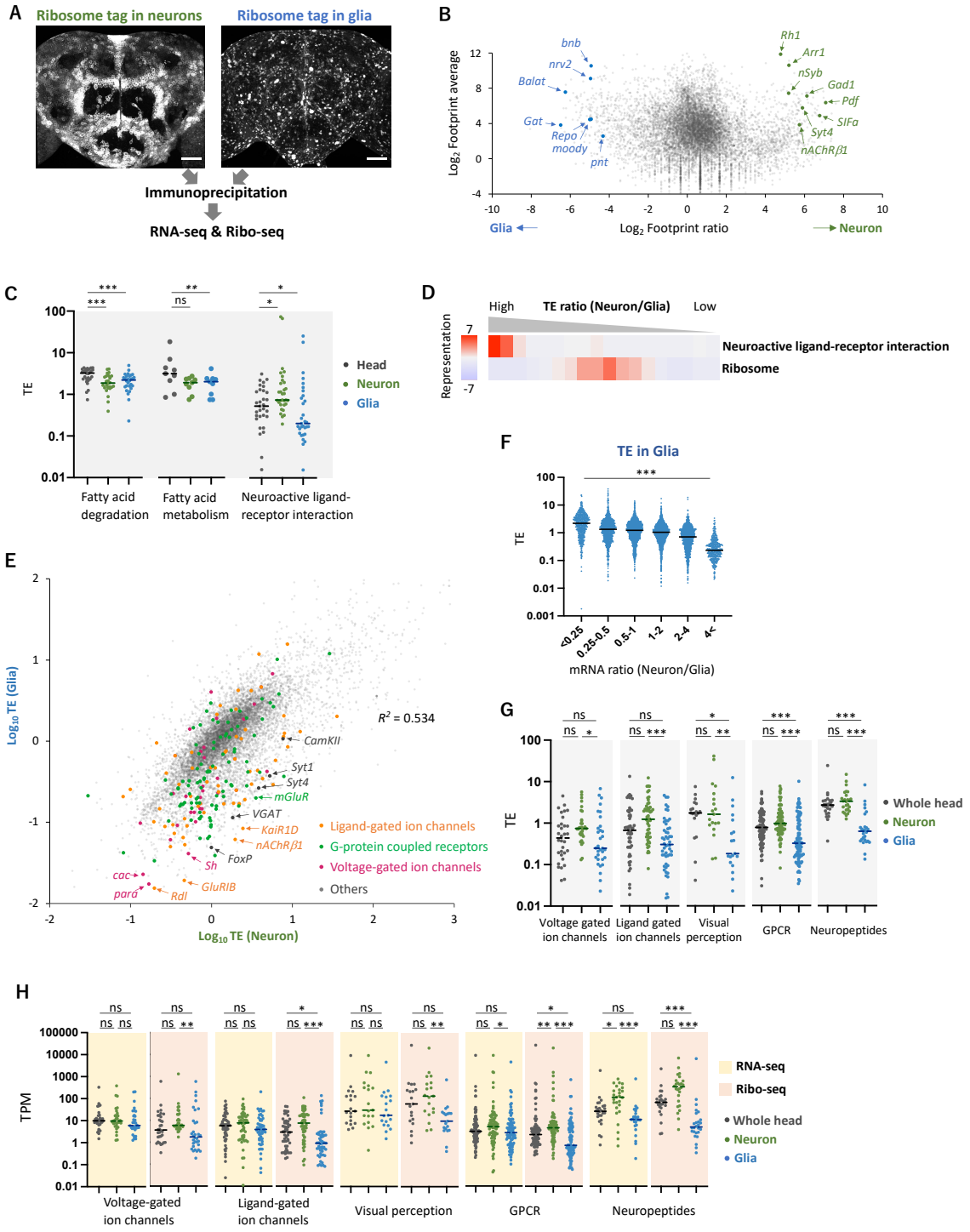

Figure 2. Cell-type specific Ribo-seq and RNA-seq reveal differential translational regulations.

(A) Schematics. FLAG-tagged ribosome protein L3 (RpL3::FLAG) is expressed in neurons (*nSyb-GAL4*) or in glial cells (*repo-GAL4*). RNA-seq and Ribo-seq are performed following

784 immunoprecipitation. Whole brain images of the exogenously expressed RpL3::FLAG are
785 shown. Scale bars: 50 μm. (B) The MA-plot of ribosome footprints on CDS among neurons
786 and glia. Each gene is plotted according to the fold change (x-axis) and the average (y-axis)
787 in the unit of $\log_2$. Several marker genes are highlighted with green (neuron) or blue (glia). (C)
788 TE of genes in the denoted KEGG pathways in the whole head (black), neurons (green), or in
789 glia (blue). Genes with TPM > 1 in the RNA-seq dataset are plotted. Bars represent the
790 median. *: $P < 0.05$, **: $P < 0.01$, ***: $P < 0.001$, the Dunn's multiple comparisons test. (D)
791 KEGG pathway enrichment analysis based on the ratio of TE in neurons to in glia. All genes
792 with at least one read in both cell types (total 9,732 genes) are ranked and binned according
793 to the neuron-to-glia ratio (left to right: high to low), and over- and under- representation is
794 tested. The presented KEGG pathways show *P* values smaller than 0.0005. (E) Scatter plot of
795 TE in neurons (x-axis) and in glia (y-axis). The squared Pearson's correlation coefficient (R^2)
796 is indicated. (F) TE in glia plotted according to the ratio of mRNA expression in neurons
797 compared to glia. ***: $P < 0.001$, Kruskal-Wallis test. All the 7,933 genes showing TPM > 1 in
798 RNA-seq are analyzed. (G) TE of transcripts, showing at least one read, in the indicated gene
799 ontology (GO) terms. Bars represent the median. **: $P < 0.01$, ***: $P < 0.001$, Dunn's multiple
800 comparisons test. (H) Read counts of genes (TPM) in the indicated GO terms in RNA-seq
801 (yellow) and in Ribo-seq (pink). The grey, green and blue dots indicate the read counts in the
802 whole head, neurons and glial cells, respectively. ns: $P > 0.05$, **: $P < 0.01$, ***: $P < 0.001$,
803 Dunn's multiple comparisons test.
804

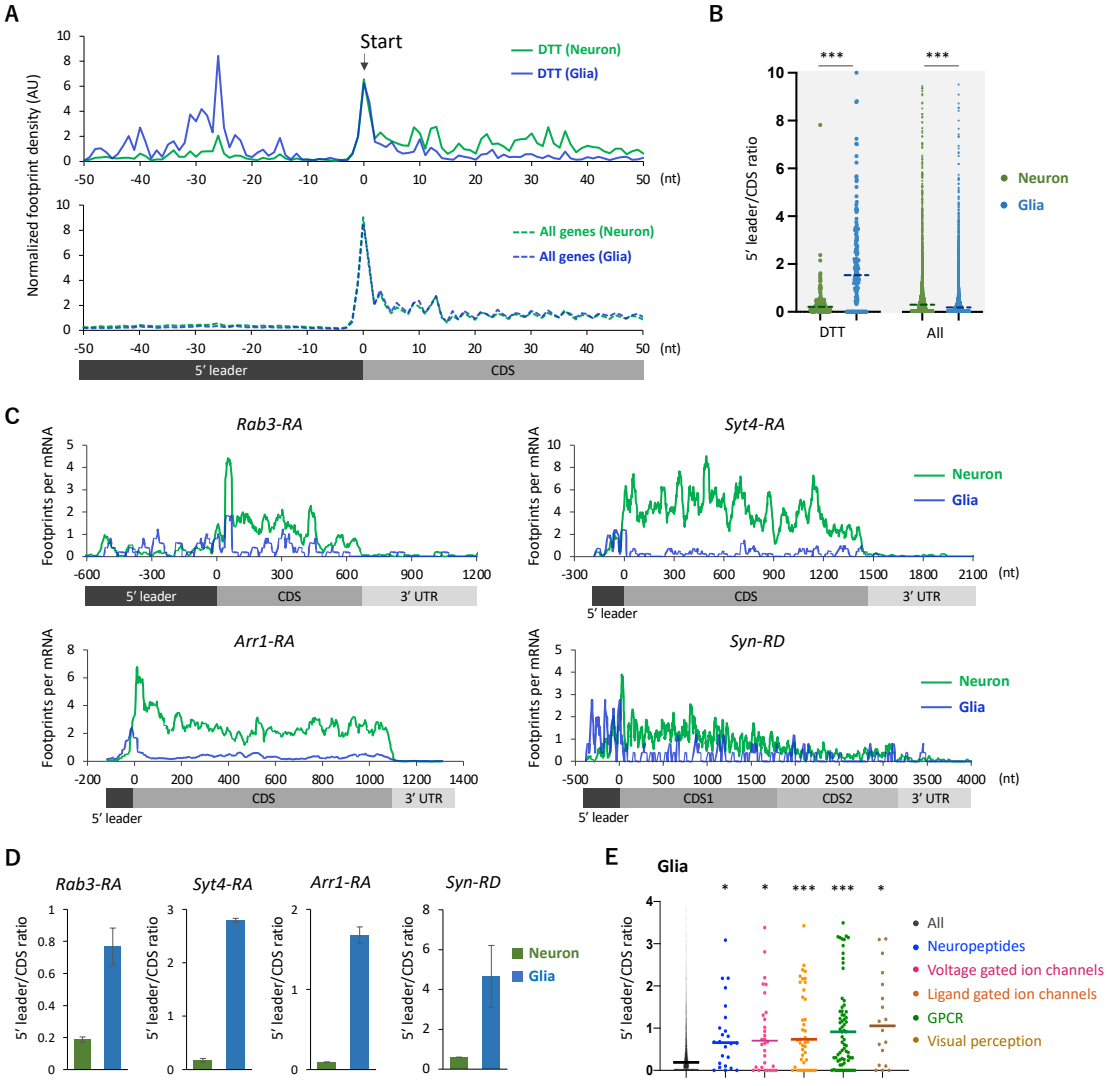

Figure 3. Ribosome stalling on the 5′ leaders of DTTs in glia.

(A) Ribosome distribution (estimated P-sites) on the 161 DTTs around the start codons (solid lines; start +/- 50 nt). These DTTs are defined as transcripts showing more than 10 times higher TE in neurons compared to glia. The dotted lines in the bottom graph indicate the genome-wide distribution. All the transcripts showing TPM > 1 in RNA-seq both in neurons and glia are considered (7,933 genes in total), and the height is normalized by the total reads on this region. (B) Ratio of ribosome density on 5′ leader (TPM) to CDS (TPM) of the 161 DTTs or of all transcripts in neurons (green) or in glia (blue). The bars represent the median. ***: $P < 0.001$, Mann-Whitney test of ranks. (C) Distribution of ribosome footprints on the representative neuronal transcripts. Ribosome footprints (RPM) normalized by the mRNA level

816 (TPM) are shown. Note that *Syn-RD* harbors a stop codon in the CDS but a fraction of
817 ribosomes skip it, generating two annotated ORFs (CDS1 and CDS2) (Klagges et al., 1996).
818 (D) Ratio of ribosome density on 5′ leader to CDS (mean ± standard error of mean of the
819 biological replicates). (E) Ratio of ribosome density on 5′ leader to CDS on transcripts in the
820 indicated GO terms in glia. *: $P < 0.05$, ***: $P < 0.001$, Dunn's multiple comparisons test
821 compared to the "all" group.
822

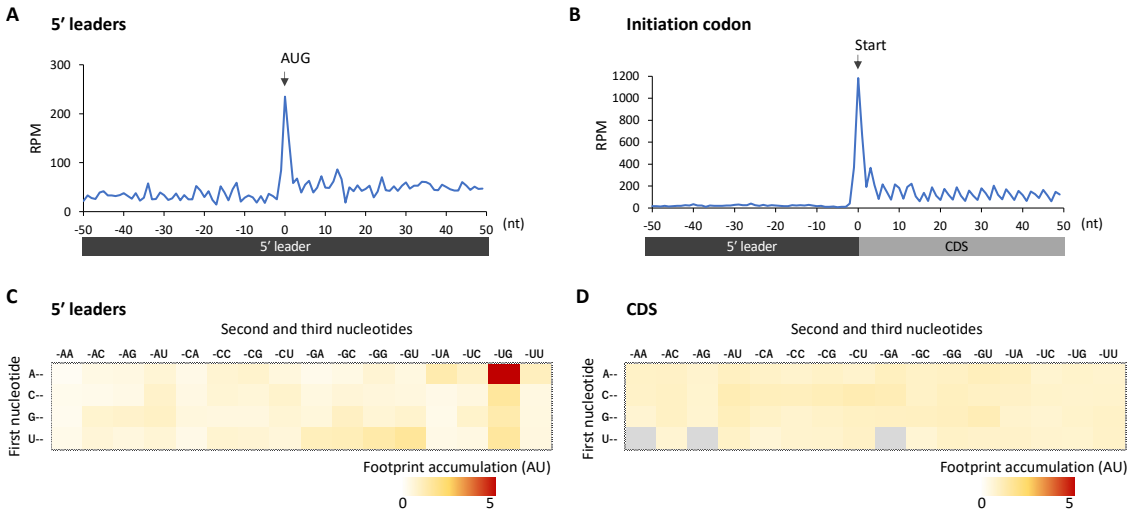

Figure 4. Footprint accumulation on upstream AUG in glia.

(A) Meta-genome ribosome distribution (estimated P-sites of the 32-nt fragments) around the upstream AUG codons in glia. (B) Meta-genome ribosome distribution (estimated P-sites of the 32-nt fragments) around the annotated start codons in glia. (C) Footprint accumulation on 5′ leader in glia, defined as the number of ribosome footprints (estimated P-sites) on each codon normalized by the average on the surrounding (-50 to +50) regions. (D) Footprint accumulation inside the annotated CDS in glia. Annotated in-frame codons except the start and the stop codons are considered. AU: arbitrary unit.

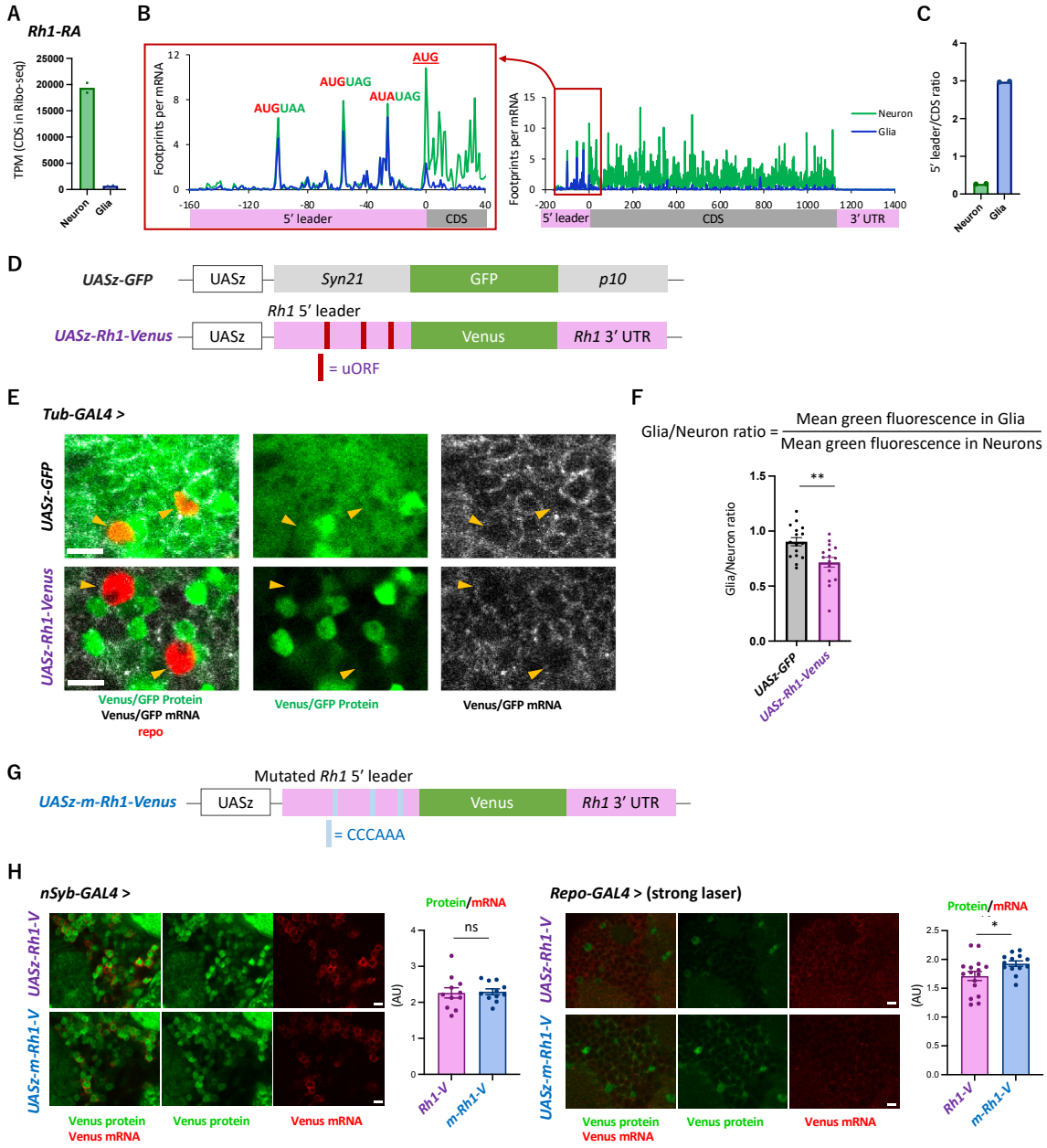

Figure 5. The transgenic *Rh1-Venus* reporter reveals differential translation in neuronal and glial cells.

(A) Reads on CDS of *Rh1-RA* in Ribo- seq. (B) Ribosome distribution (estimated P-sites) on *Rh1-RA* in neurons (green) and in glia (blue), with 0 on the x-axis indicating the start codon of the CDS. 6-base upstream ORFs, consisting of consecutive start (or the near-cognate) and stop codons, are highlighted. Note that footprints are normalized by the mRNA level (TPM). (C) Ratio of ribosome density on 5′ leader (TPM) to CDS (TPM) in neurons (green) or in glia (blue). The bars and the dots represent the median and individual data points, respectively.

842 (D) Schematics of the control (*UASz-GFP*) or the *Rh1* (*UASz-Rh1-Venus*) reporter. For the
843 *Rh1* reporter, 5′ leader and 3′ UTR sequences of *Rh1-RA* are fused to CDS of the *Venus*
844 fluorescent protein. For the control reporter, synthetic 5′ leader sequences (*syn21*) and viral
845 *p10* terminator are fused to GFP (DeLuca and Spradling, 2018). Note that both reporters
846 contain the same promoter (*UASz*) (DeLuca and Spradling, 2018) and are inserted onto the
847 identical genomic locus (*attP40*). (E) Expression of the *Rh1*- or the control reporters driven by
848 *Tubulin-GAL4*. Sliced confocal images of the cortical regions next to the antennal lobe are
849 shown. Green: EGFP or Venus fluorescent signal. Red: Immunohistochemical signal of repo
850 protein as a glial marker. Grey: EGFP or Venus mRNA. Orange arrowheads indicate glial cells
851 marked by the repo expression. Scale bars: 5 μm. (F) Quantification of the green fluorescent
852 intensity in glial nuclei, nomalized by the fluorescence in neurons. Glial intensity was measured
853 as mean intensity in the repo-positive pixels, and was normalized by the mean intensity in the
854 repo-negative pixels. **: $P < 0.01$, Mann-Whitney test of ranks. (G) Schematics of the mutated
855 *Rh1* reporter (*m-Rh1*). The minimal uORF is replaced with CCCAAA. (H) The expression of
856 the *Rh1*- or *m-Rh1*- reporters, driven by the *nSyb*- or the *repo*- GAL4. Sliced confocal images
857 of the cortical regions next to the antennal lobe are shown. Green: Venus fluorescent signal.
858 Red: Venus mRNA signal. The total protein signal was normalized by the total mRNA signal
859 for each brain. $N = 8$ (*nSub* > *Rh1*), 8 (*nSyb* > *m-Rh1*), 16 (*repo* > *Rh1*), 13 (*repo* > *m-Rh1*).
860 ns: $P > 0.05$, *: $P < 0.05$, Mann-Whitney test of ranks.